








Open Archive Toulouse Archive Ouverte (OATAO)

OATAO is an open access repository that collects the work of Toulouse researchers and makes it freely available over the web where possible

This is an author's version published in: <http://oatao.univ-toulouse.fr/24225>

Official URL: <https://doi.org/10.1016/j.ces.2019.01.024>

To cite this version:

El Hage, Ranine  and Chauvet, Fabien  and Biscans, Béatrice  and Cassayre, Laurent  and Maurice, L. and Tzedakis, Théo  *Kinetic study of the dissolution of vanadyl sulfate and vanadium pentoxide in sulfuric acid aqueous solution.* (2019) *Chemical Engineering Science*, 199. 123-136. ISSN 0009-2509

Any correspondence concerning this service should be sent to the repository administrator: tech-oatao@listes-diff.inp-toulouse.fr

Kinetic study of the dissolution of vanadyl sulfate and vanadium pentoxide in sulfuric acid aqueous solution

R. El Hage^a, F. Chauvet^a, B. Biscans^b, L. Cassayre^b, L. Maurice^c, T. Tzedakis^{a,*}

^aLaboratoire de Génie Chimique, UMR CNRS 5503, CAMPUS Université Toulouse III – Paul Sabatier, FSI, 118, Route de Narbonne, 31062 Toulouse, France

^bLaboratoire de Génie Chimique, UMR CNRS 5503, CAMPUS INP – ENSIACET, 4 allée Emile Monso, 31 432 Toulouse, France

^cUniversité Toulouse III – Paul Sabatier, 118, Route de Narbonne, 31062 Toulouse, France

H I G H L I G H T S

- Vanadium (IV) sulfate VO_2SO_4 and vanadium (V) pentoxide V_2O_5 dissolution.
- Temporal evolution of the concentrations of VO^{2+} and VO_2^+ at various temperatures.
- Understanding the dissolution limitations: $\text{V}^{\text{IV}} \rightarrow$ mass transfer; $\text{V}^{\text{V}} \rightarrow$ reaction with H^+ .
- Simple kinetic models to predict the evolution of VO^{2+} and VO_2^+ concentrations.

A R T I C L E I N F O

Keywords:

Vanadyl sulfate
Vanadium pentoxide
Dissolution kinetics
Vanadium redox battery
Solubility

A B S T R A C T

The study deals with the ‘vanadium (IV) sulfate’ and ‘vanadium (V) pentoxide’ dissolution processes in 3 M H_2SO_4 aqueous media. Several measurements of the concentration of dissolved VO^{2+} and VO_2^+ were achieved in the range of 0–40 °C, and allowed to understand the limitations of the dissolution process (‘endothermic’ mass transport for VO_2SO_4 and ‘exothermic’ reaction with the proton for V_2O_5). In addition, simple models were proposed (diffusion/accumulation for VO_2SO_4 and kinetic rate for V_2O_5) and their resolution leads to theoretical kinetic equations describing the temporal evolution of these concentrations with satisfactory agreement with the experimental curves. Solubility’s data and their temperature dependence were determined for both vanadium compounds involved.

1. Introduction

Renewable energy storage studies have expanded in the past decades due to the rapid increase in energy consumption, limited fossil fuels reserves and growing ecological concerns of their impact on health and environment.

Only a very limited number of systems enable energy storage such as thermal storage, pumped hydropower and compressed air energy storage (Amirante et al., 2017; Ding et al., 2009). Electrochemical storage constitutes an interesting alternative and recently the Redox Flow Battery (RFB) acquired a great importance as they have the particularity of converting and storing energy by using electroactive species dissolved in electrolyte solutions (Wang et al., 2013; Leung et al., 2012). The most spread RFB is the “all

vanadium” redox flow battery (VRFB) developed in the 1980’s by Rychcik and Skyllas Kazacos (1988), Skyllas Kazacos et al. (1988) and has been widely explored since (Cunha et al., 2015; Skyllas Kazacos et al., 2016, 2015, 2013).

The battery was introduced to overcome the problem of cross contamination of electrolytes, inducing capacity losses reported primarily by NASA researches in the 1970s for the Fe–Cr system (Thaller, 1977, 1974). Given that the same element in different oxidation states is used in both compartments of the VRFB, no contamination of the active material will occur in case ions cross the ionic separator. The redox couples employed are $\text{V}^{\text{III}}/\text{V}^{\text{II}}$ and $\text{V}^{\text{V}}/\text{V}^{\text{IV}}$ for the negative and the positive half cells respectively (Sum et al., 1985; Sum and Skyllas Kazacos, 1985), and the only redox reactions involved are thus the valence changes of the vanadium ions. The electrolyte solutions are usually prepared in 2–3 M sulfuric acid, even if other electrolytes have been investigated (generation 2 and 3 of the VRB) (Skyllas Kazacos et al., 2007). The VRB is characterized by a long life span (>10,000 cycles) (Ashby and Polyblank, 2012), low maintenance cost and deep discharge

* Corresponding author at: Chemical Engineering Laboratory, UMR CNRS 5503, FSI, Université Toulouse III – Paul Sabatier, 118, Route de Narbonne, 31062 Toulouse, France.

E-mail address: tzedakis@chimie.ups-tlse.fr (T. Tzedakis).

Nomenclature

$A_{(765\text{ nm})}$	absorbance at the wave length of 765 nm	PES	polyether sulfone
A	Arrhenius pre exponential factor	R°	initial radius of the particle (m)
$a_{\text{VOSO}_4\text{ solid}}$	activity of the solid compound	$R_{(t)}$	radius of the particle at the dissolution time t (m)
a	constant (Leveque correlation)	r°	initial reaction rate (mol L ⁻¹ s ⁻¹)
A_1, A_2, A_3 and A_4	constants (defined in Appendix A)	r_{global}	total rate of the reaction of the dissolution of V ₂ O ₅ (mol L ⁻¹ s ⁻¹)
C_{bulk}	concentration of VO ²⁺ in the bulk (M)	RFB	Redox Flow Battery
C_{surface}	$C_{\text{saturation}}$ superficial concentration of VO ²⁺ , assumed at saturation (M)	Re	Reynolds number $\frac{d_p \times \bar{u}}{\nu}$ $d_p \times \bar{u} \times \frac{\rho}{\mu}$
d_p	particle diameter at time t (μm)	SEM	scanning electron microscope
D	diffusion coefficient (m ² /s)	S	surface of particles involved in the dissolution process (m ²)
E_a	activation energy (J/mol)	Sc	Schmidt number = ν/D
$e_{(t)}$	thickness of the spherical crown film, function of the time (m)	Sh	Sherwood number $(Sh = \frac{k_{(t)} \times d_p}{D})$
ϵ	absorptivity (cm ⁻¹ M ⁻¹)	t	dissolution time (expressed in 's' for VOSO ₄ and in 'h' for V ₂ O ₅)
$\Delta_R H$	reaction enthalpy (J/mol)	\bar{u}	average rate of the liquid around the solid particle calculated from the stirring rate (m/s), assumed constant during the experiment time
j	number of iterations taken as 100	ν	kinematic viscosity (m ² /s) μ/ρ
k	kinetic constant following the Arrhenius law (unit function of the reaction order)	ΔU	internal energy (J/mol)
$k_{(t)}$	$\frac{D}{e_{(t)}}$ mass transfer coefficient of the VO ²⁺ around the solid particle of VOSO ₄ (m ⁻¹ s)	VRFB	Vanadium Redox Flow Battery
m	moles number of dissolved VOSO ₄ (to VO ²⁺) into the bulk	V	solid volume present in the solution at time t (m ³)
M	molar mass of the solid VOSO ₄ 5H ₂ O (kg/mol)	V_l	total volume of the solution (including both the liquid and the powder)
N	number of VOSO ₄ particles having a certain initial radius R°	ω	stirring rate (rpm)
$n^{\circ}_{(V)}$	initial moles number of V ₂ O ₅ (mol)	X	moles number of V ₂ O ₅ dissolved at time t
$n^{\circ}_{(H)}$	initial moles number of H ⁺ (mol)		
ρ	specific gravity of the powder (kg/m ³)		
PTFE	polytetrafluoroethylene		

capability (Vijayakumar et al., 2013). The energy density of the battery is largely depending on the volume and concentration of the vanadium electrolytic solutions and numerous authors studied the effect of the composition of electrolyte solutions (Choi et al., 2017; Skyllas Kazacos et al., 2016) on the performance of the battery.

Despite that, stable solutions with vanadium concentrations higher than 2 M could not be achieved in the working conditions of the VRB, limiting the quantity of stored energy to around 40 kWh/m³.

The electrolyte in the negative electrode compartment does not seem to exhibit major limitations related to the solubility of V^(III) and V^(II), but one point to mention is that V^(II) is easily oxidized by air (choi et al., 2013). One important limitation encountered by the vanadium battery appears to be related to the precipitation of compounds in the positive electrode: precipitation of the V^(IV) at low temperature and precipitation of the V^(V) compounds at high temperature.

This fact limits the working temperature range of the VRB between 10 and 40 °C (Li et al., 2011). Precipitation of various vanadium salts and oxides was studied by several research groups and it was found that higher sulfuric acid concentrations stabilizes the V^(V) solutions (Rahman, 1998) but decreases the solubility of V^(II), V^(III) and V^(IV). This is attributed to the common sulfate ion effect (Skyllas Kazacos et al., 2016): increasing the total sulfate concentration shifts the equilibria (1)–(4) towards the left, leading to a lesser dissociation of the vanadium sulfate salts (Rahman and Skyllas Kazacos, 1998; Cheng, 1991) and to the precipitation of the salts in solution.



As mentioned by Rahman and Skyllas Kazacos (2009), vanadium (V) can precipitate after 1000 h at 50 °C and the redissolution of the oxide V₂O₅ (Rahman, 1998) appears to be difficult. Numerous authors (Ivakin and Voronova, 1973; Vijayakumar et al., 2011; Kausar, 2002) conducted studies to understand the poor thermal stability of V^(V) at high temperatures. They showed that the precipitation process of V₂O₅ is endothermic and thus enhanced when temperature increases.

Moreover, the aqueous chemistry of vanadium (V), studied by several authors (Crans et al., 2004; Elvingson et al., 1998), inferred the presence of many species as a function of the solution's pH. It was suggested that pervanadyl or dioxovanadium cation (VO₂⁺) is the main species formed in the lower pH range (0.5–1.3) (Baes and Mesmer, 1976). However, the presence of VO₃ species was also reported in the concentration range of 1 M of V^(V) in 5 M total sulfate (Kausar, 2002). Based on Raman spectroscopy analysis, the authors propose that VO₃ species are surrounded by a densely packed ionic environment of other V^(V) and sulfate ions and these ions could be involved in weak or unstable complex formation with other ions. In the case of H⁺ ions depletion, VO₃ tends to precipitate as a disordered V₂O₅ aggregate (Kausar, 2002). Increasing the acid concentration enables to prevent this precipitation and favor the stabilization of V^(V) in the form of VO₂⁺. However, this induces a negative effect on the overall performance of the battery because of the increasing viscosity and an enhancement of the ohmic drops resulting in the lowering of the energy efficiency (Choi et al., 2017).

Numerous works exist on the field of the vanadium battery, and one important objective is to avoid the vanadium pentoxide

precipitation. Indeed according to [Rahman \(1998\)](#) and [Rahman and Skyllas Kazacos \(2009\)](#) vanadium (V) oxide dissolution is difficult, in addition to being an endothermic dissolution ([Ivakin and Voronova, 1973](#); [Vijayakumar et al., 2011](#); [Kausar, 2002](#)). Neither the understanding of the dissolution phenomena of the vanadium compounds, nor elucidation of the corresponding mechanisms was significantly explored; the published studies do not exhibit the determination of the physical limitations in order to act upstream. Hence, the present work deals with the study of the dissolution mechanisms of two common vanadium compounds in 3 M sulfuric acid, at various temperatures (0–40 °C), stirring rates and initial particles size. Apart from being the most common concentration used for an operating battery with 2 M VOSO₄, the sulfuric acid concentration (3 M) is chosen here, as a compromise between its positive effect on the dissolution of the vanadium pentoxide and its negative effect on the dissolution of vanadium sulfate ([Rahman, 1998](#)). Note also that, by increasing the sulfuric acid concentration, the solubility of the oxide increases, but this increases the viscosity of the solution leading to a pressure drop. Moreover, during the cycling of the battery and more specifically during recharge (oxidation of V^(IV) to V^(V)), H⁺ ions are generated in the positive compartment leading to an increase in acidity, therefore, it is not necessary to study higher H₂SO₄ concentrations.

To sum up, the general purpose of this study is to understand the phenomena governing the dissolution of vanadyl sulfate VOSO₄ and vanadium pentoxide V₂O₅ and to establish the corresponding kinetic laws, in order to have a better control on the accidental precipitation during VRB operations.

2. Material and methods

2.1. Dissolution protocol

The chemicals used are vanadium (IV) sulfate oxide hydrate VOSO₄·xH₂O (99.9%), vanadium (V) pentoxide V₂O₅ (99.6%) from Alfa Aesar, NormaPur H₂SO₄ from Sigma Aldrich, and deionized water.

Dissolution experiments were achieved in a thermo regulated reactor (cylinder of an internal diameter = 2 cm) at constant temperature. An adequate volume of aqueous solution 3 M sulfuric acid is poured in the reactor and stirred with a 1.5 cm magnetic bar until reaching the selected temperature. Then, an excess of vanadium compound is added ($m_{(\text{vanadyl sulfate})} = 4.559 \text{ g}$ and $m_{(\text{vanadium pentoxide})} = 1.461 \text{ g}$), marking the initial time of the experiment. Stirring rate is kept constant during the experiment. At regular time intervals, aliquots are withdrawn from the solution with plastic syringes and are directly filtered twice with filters resisting to the acid media. The first filtration is performed using a polyether sulfone (PES) filter with a pore diameter of 0.23 μm, and the second one a polytetrafluoroethylene (PTFE) membrane filter (Millipore ready to use filters in plastic assembly) with a pore diameter of 0.1 μm.

The recovered filtrate is diluted and analyzed with the appropriate method.

The vanadium compounds dissolution occurs according to reactions (3) and (5) for VOSO₄ and V₂O₅ respectively.



These reactions were taken into account because the species involved at the chosen concentration of H₂SO₄ (3 M) are in agreement with the E-pH diagram indicated by [Post and Robins \(1976\)](#), and with the V^(V) species distribution calculated from constants given by [Baes and Mesmer \(1976\)](#), [Guzman et al. \(2002\)](#).

2.2. Characterization methods

2.2.1. UV visible spectrophotometry for vanadium (IV) analysis

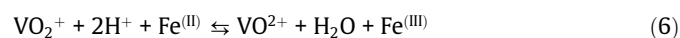
The UV VIS spectrophotometer device is a Hewlett Packard Model 8453.

According to their oxidation state, the vanadium compounds exhibit various absorption bands at the UV visible wavelengths range. However, no absorption band could be determined for the VO₂⁺ species; this is why potentiometric titration was used (see next section).

For the V^(IV) quantification, the absorbance was measured at a wavelength of 765 nm ([Choi et al., 2017](#)) exclusively due to VO²⁺. A preliminary calibration enables to obtain the A_(765nm) = f([VO²⁺]) correlation and leads to an absorptivity ε value of 21.4 cm⁻¹ M⁻¹, with deviations $\frac{\Delta \epsilon}{\epsilon}$ of 0.6 and 0.25 from the values proposed by [Choi et al., 2013](#) and [Brooker et al. \(2015\)](#) respectively.

2.2.2. Potentiometric titration of vanadium (V)

A potentiometric titration method is used to determine the concentration of the VO₂⁺ released from the dissolved V₂O₅ powder. The titration agent is Mohr salt, supplied by Sigma Aldrich and prepared in sulfuric acid media ([Le Flem, 1964](#)). The redox systems involved in this titration are thus VO₂⁺/VO²⁺ and Fe^(III)/Fe^(II) and the titration reaction is:



The titrations are carried out using a combined Pt-Ag/AgCl/Cl electrode.

2.2.3. ICP analysis

ICP analysis (Inductively Coupled Plasma; ULTIMA 2 ICP-OES) was used for total vanadium aqueous concentration determination, in order to characterize the amount of water in the commercial vanadyl sulfate powder VOSO₄·xH₂O.

2.2.4. Morphology and particle size distribution of the powders

The scanning electron microscope (SEM) used to observe the grains morphology is a PhenomWorld XL SEM. The solid powders (V₂O₅ and VOSO₄·xH₂O) were coated with a thin gold layer (using an Emiteck K550X device) prior SEM observation.

A laser diffraction particle sizing technique, using a Malvern Mastersizer 3000, was used to get the size distribution of the grains. The Malvern Mastersizer is usually used for materials ranging from hundreds of nanometers to several millimeters in size ([Fu and Sun, 2001](#)). The particle size is reported as a volume equivalent sphere diameter.

3. Results and discussion

3.1. Dissolution of vanadium (IV) sulfate

3.1.1. Characterization of the initial powder

The commercial vanadyl sulfate powder VOSO₄·xH₂O used for the dissolution experiments is partially hydrated. Its water content x was determined by ICP at different concentrations, according to the method of determination of the vanadium concentration in an aqueous solution. The results of three analyses are found to be in the range from 5.4 to 5.6; thus taking into account the uncertainties of the analyses, the retained value of x is 5. Note that this result is in agreement with an octahedral geometry, and also with the fact claimed by [Selbin \(1965\)](#), the hydrated vanadyl sulfate exists as [VO(H₂O)₅]²⁺, 'the vanadyl ion' in acidic solutions. In the following, VOSO₄·xH₂O is thus indicated as VOSO₄·5H₂O [Fig. 1](#).

[Fig. 1](#) presents SEM micrographs of the commercial powder. These images display aggregated and multi-shaped particles of

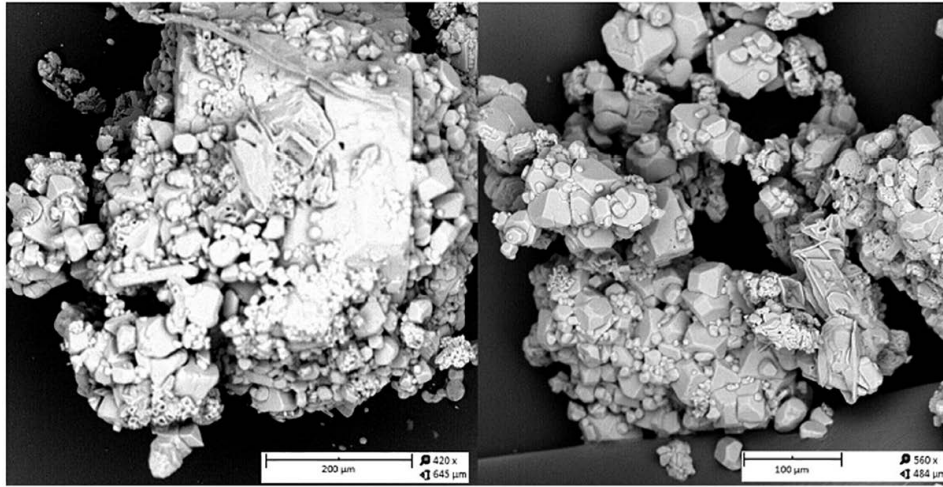


Fig. 1. SEM images of the vanadyl sulfate $\text{VOSO}_4 \cdot 5\text{H}_2\text{O}$ commercial powder; 15 kV-Point; BSD full.

all sizes. Their dispersion during the dissolution in a stirred solution is expected to be easy, because of the dislocation occurring after the dissolution of the smallest particles.

The $\text{VOSO}_4 \cdot 5\text{H}_2\text{O}$ particle size distribution is presented in Fig. 2. The first graph (Fig. 2 1) provides the particle size distribution of the commercial powder and clearly shows two distinct ranges: from 5 to 350 μm and from 350 μm to 4 mm. The commercial powder was sieved at 315 μm and separated into two fractions, for which particle sizes are presented in Fig. 2 2 and 3. They confirm two distinct populations of particle diameter: $d_p < 315 \mu\text{m}$ and $d_p > 315 \mu\text{m}$.

3.1.2. Temperature dependence of the dissolution kinetics

Fig. 3 gathers experimental measurements of VO^{2+} concentration in the electrolyte during the dissolution, for temperatures in the range from 5 to 30 $^\circ\text{C}$. For all the examined temperatures, a similar temporal evolution of the concentration of VO^{2+} was observed: the concentration increases rapidly at short reaction times ($t < 3 \text{ min}$) and then the dissolution slows down until equilibrium is reached, after around 10 min. When the temperature increases from 5 to 30 $^\circ\text{C}$ the initial dissolution rate increases as well.

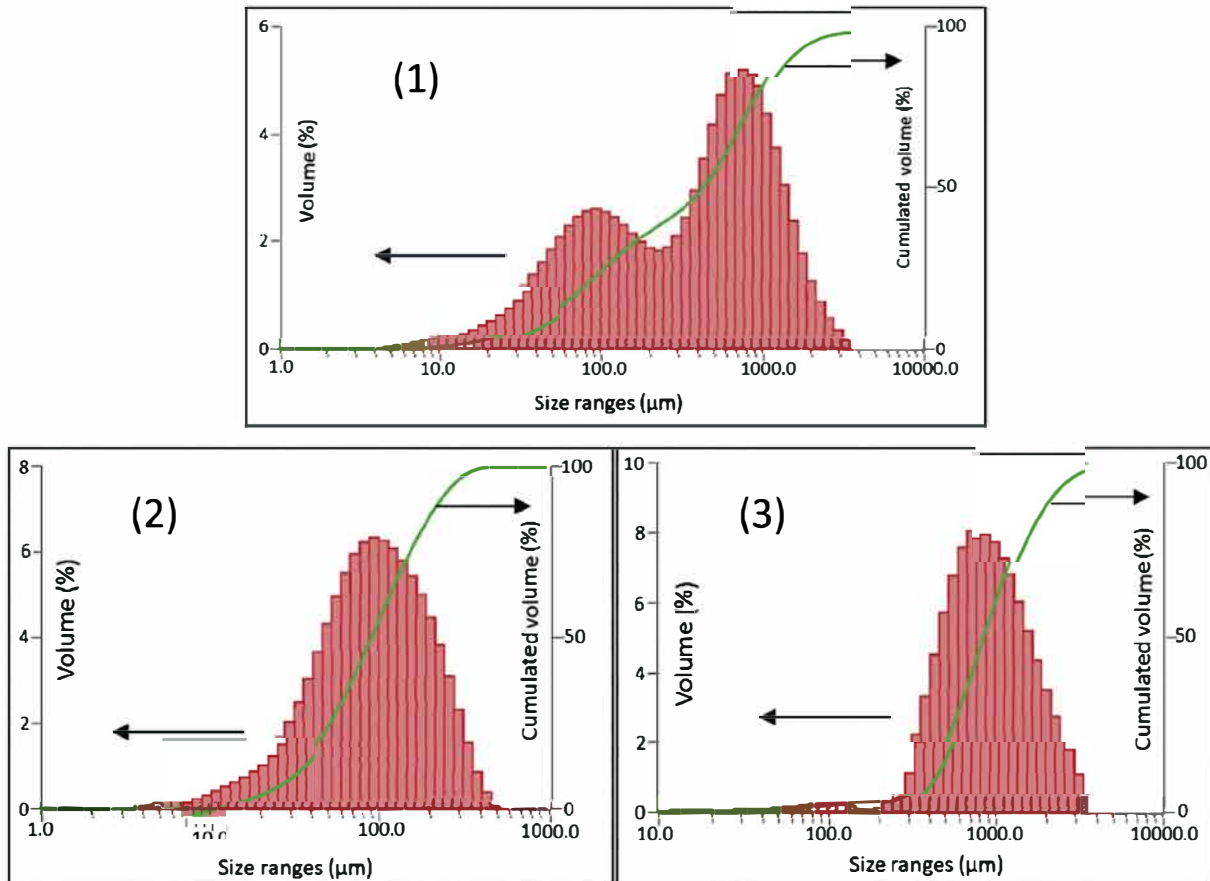


Fig. 2. Laser diffraction analysis ($P = 3 \text{ bar}$; dry mode) showing the $\text{VOSO}_4 \cdot 5\text{H}_2\text{O}$ size distribution: (1) commercial powder; (2) sieved powder $d_p < 315 \mu\text{m}$; (3) sieved powder $d_p > 315 \mu\text{m}$.

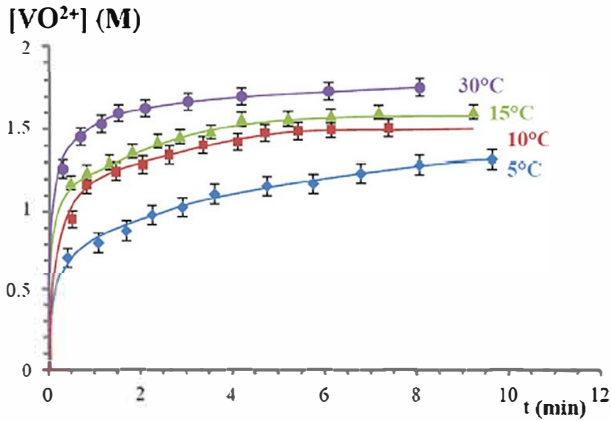


Fig. 3. Temporal evolution of the concentration of VO^{2+} released by the dissolution of a $\text{VOSO}_4 \cdot 5\text{H}_2\text{O}$ commercial powder, for various temperatures; $[\text{H}_2\text{SO}_4] = 3 \text{ M}$; stirring 500 rpm; aliquots filtered by 0.23 and 0.1 μm filters.

The first concentration reported on the graph corresponds to 20 s after the introduction of the solid into the stirred solution. For this first measurement, at 5 °C the vanadium concentration reaches 0.7 M and this value doubles (1.3 M) at 30 °C.

The concentration of the VO^{2+} measured at 20 s, will be used to determine the initial dissolution rate r° (defined as the ratio $\frac{[\text{VO}^{2+}]_{20\text{s}}}{20\text{s}}$). Assuming that the kinetic constant of the initial dissolution rate follows the Arrhenius law, Eq. (1) gives the initial dissolution rate r° .

$$r^\circ = k \times f \times A \times e^{-E_a/RT} \times f \quad (1)$$

where f is a function of the various operating parameters (activity of the solid vanadyl sulfate, diffusion coefficient of VO^{2+} , size of solid particles. . .). Some of these parameters depend on the temperature and this dependence is expected to be studied in a future work. Here, in order to get a rough order of the magnitude of the activation energy, the experimental data were analyzed (assuming the function f independent of T) and leads to the following linear regression:

$$\ln r^\circ \left(\frac{\text{M}}{\text{s}}\right) = \frac{2266.7}{T(\text{K})} + 4.8579 \quad (2)$$

This relation leads to an approximation of the activation energy of 18.8 kJ/mol for the dissolution of $\text{VOSO}_4 \cdot 5\text{H}_2\text{O}$ in 3 M sulfuric acid, a value relatively low compared to the activation energy of a classical chemical reaction.

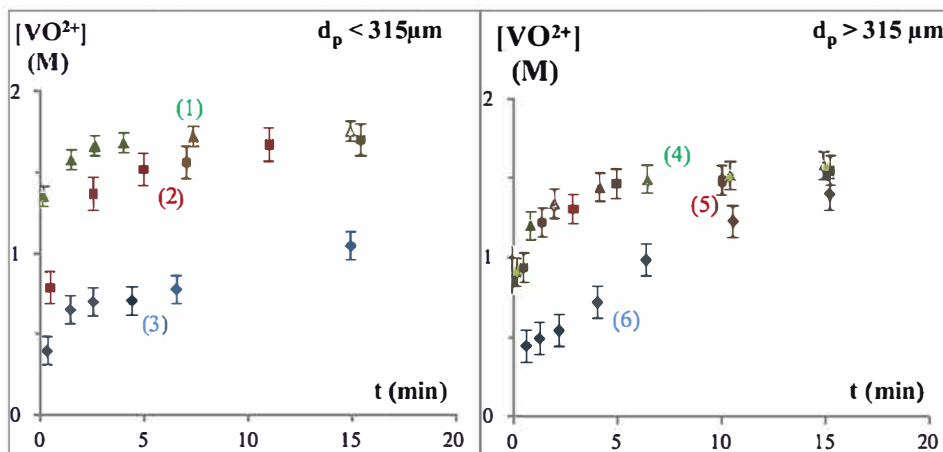


Fig. 4. Temporal evolution of the concentration of VO^{2+} released by the dissolution of a $\text{VOSO}_4 \cdot 5\text{H}_2\text{O}$ commercial powder, for suspensions containing two different particle sizes and subjected to various stirring rates ω . $T = 25 \text{ }^\circ\text{C}$, $[\text{H}_2\text{SO}_4] = 3 \text{ M}$, $\text{VOSO}_4 \cdot 5\text{H}_2\text{O}$ powder; Left: $d_p < 315 \mu\text{m}$: ω (in rpm) for (1), (2) and (3) are 500/triangles, 100/squares and 15/diamonds respectively; Right: $d_p > 315 \mu\text{m}$: ω (in rpm) for (4), (5) and (6) are 500/triangles, 100/squares and 15/diamonds respectively.

3.1.3. Effect of stirring rate and particle size on dissolution kinetics

Several dissolution experiments were achieved by applying three stirring rates (500, 100 and 15 rpm), corresponding respectively to (i) a well stirred homogeneous suspension, (ii) a minimum stirring rate enabling to uplift the particle and (iii) partially decanted solid. Besides, these experiments were carried out for two different particles size d_p ($< 315 \mu\text{m}$ and $> 315 \mu\text{m}$). The corresponding time evolution of VO^{2+} concentration is presented in Fig. 4.

For a defined range of particles size ($d_p < 315 \mu\text{m}$ curves 1 2 3 or $d_p > 315 \mu\text{m}$ curves 4 5 6, Fig. 4), it appears that a higher stirring rate increases the dissolution kinetics, since higher concentrations are achieved in a shorter time. For instance, $[\text{VO}^{2+}]_{(d_p < 315 \mu\text{m}; \omega = 500 \text{ rpm}; t = 1')} = 1.5 \text{ M}$ and $[\text{VO}^{2+}]_{(d_p < 315 \mu\text{m}; \omega = 100 \text{ rpm}; t = 1')} = 1.0 \text{ M}$.

Under constant stirring, the dissolution rate increases by decreasing the particles size. Thus, for a given dissolution time, and before reaching equilibrium, higher salt concentrations were measured with smaller particles. Indeed comparison of curves (1) and (4) obtained in two "well stirred" suspensions show that the concentration of VO^{2+} after 1 min reaction time increases from ~ 1.2 to $\sim 1.5 \text{ M}$ when the size decreases from $d_p > 315 \mu\text{m}$ to $d_p < 315 \mu\text{m}$.

A different shape is obtained for curves (3) and (6), which corresponds to the lowest stirring rate; they exhibit the slowest dissolution rate for both particle sizes. The slow agitation does not enable the motion of the particles which sediment at the bottom of the vessel, forming a 'coagulated' powder paste. Around each grain of this paste, the VO^{2+} concentration reaches rapidly the saturation concentration. These facts are in agreement with a dissolution rate limited by mass transfer. For long reaction time, all the curves tend to converge to the same saturation concentration (~ 1.7 to 1.8 M).

3.1.4. Equilibrium data

After a certain time of stirring (between 5 and 10 min), the solution is saturated and the concentration of VO^{2+} is constant. The equilibrium values are reported in Fig. 5, along with data from Skyllas Kazacos et al. (2016) and Rahman and Skyllas Kazacos (1998).

A satisfactory agreement is observed between our results and those of previous works, which confirms that the solubility of VO^{2+} increases with temperature. For the highest comparable temperature (30 °C), a significant difference of around 20% is observed.

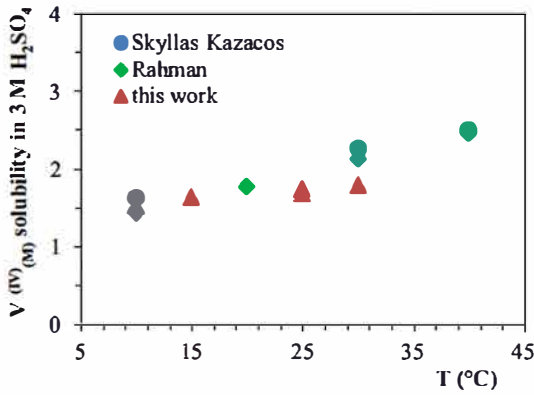


Fig. 5. Influence of temperature on the solubility of $V^{(IV)}$. Triangles: this work; circles: M. Skyllas-Kazacos et al.; diamonds: F. Rahman et al.

This could be attributed to the difficulties encountered in the measurement of a precise volume at this temperature.

The results show that the solubility of VO^{2+} increases with temperature. The equilibrium constant of the $VOSO_4 \cdot 5H_2O$ dissolution (reaction (3)) can be written as following:

$$K_{(3)} = \frac{(a_{VO^{2+}} \times a_{SO_4^{2-}})}{a_{VOSO_4 \text{ solid}}} \text{ at the equilibrium} \quad (3)$$

Even if the first dissociation of H_2SO_4 to HSO_4^- is total (high $K_{H_2SO_4/HSO_4^-}$), the second dissociation to SO_4^{2-} remains partial with an equilibrium constant $K_{HSO_4^-/SO_4^{2-}} = 0.013$ at 25 °C (the concentrations are in mol/kg) (Wallace, 1966). However, the released quantity of sulfate ions from HSO_4^- dissociation is not significant compared to the quantity released from the dissolution of $VOSO_4$; this imply that $[VO^{2+}]$ can be assumed equal to $[SO_4^{2-}]$.

Concerning the activity of the solid powder of $VOSO_4$, we will assume it equal to 1. Thereby, the above equation can be written as follows:

$$K_{(3)} \frac{\gamma_{VO^{2+}} \times \gamma_{SO_4^{2-}}}{a_{VOSO_4 \text{ solid}}} \times [VO^{2+}] \times [SO_4^{2-}] \Rightarrow K_{(3)} \lambda \times \left([VO^{2+}]_{\text{at equilibrium}} \right)^2 \quad (4)$$

$$\text{where } \lambda = \frac{\gamma_{VO^{2+}} \times \gamma_{SO_4^{2-}}}{a_{VOSO_4 \text{ solid}}}$$

Because the concentrations of VO^{2+} at saturation are relatively high (1.2–1.7 M), the activity coefficients depend on the concentration, while the activity of the vanadyl sulfate solid is equal to 1; in a future work, the Pitzer model will be used in order to express these activity coefficients. Here, in order to get a rough estimation of the sensitivity of vanadyl sulfate solubility against temperature, the logarithm of the VO^{2+} saturation concentration was plotted versus $1/T$, assuming λ independent from the concentration of the various species.

The linear regression analysis leads to the following relation:

$$\ln[VO^{2+}]_{\text{sat (mM)}} = \frac{982.2}{T(\text{inK})} + 3.8$$

with a relatively low correlation coefficient ($R^2 = 0.91$) with the experimental results, explaining the uncertainties due to the dependence of the activity coefficients on the concentration.

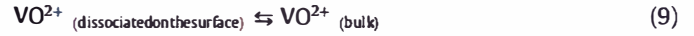
From the slope of the above equation ($982.2 \text{ kJ}/(2R)$), we deduce the value of $k = 16.3 \text{ kJ/mol}$.

The obtained value is (i) positive showing the endothermic character of the vanadyl sulfate dissolution, and (ii) a relatively low value, compatible with the dissociation of an ionic salt weakly bonded.

3.1.5. Elucidation of the mechanism of the vanadyl sulfate dissolution

The results of this study show that, at constant temperature, the dissolution of vanadyl sulfate in 3 M sulfuric acid is limited by mass transport and that two main parameters (stirring rate and particle size) affect the dissolution rate.

Let us consider the following mechanism for the dissolution of the solid salt $VOSO_4 \cdot 5H_2O$:



Taking into account the results related to the effect of stirring (§3.1.3), the limiting step in the vanadyl sulfate dissolution will be assumed to be the transport of the VO^{2+} from the surface of the particles to the bulk i.e. reaction (9). Besides, in the absence of an electric field, the transport of ions produced in reaction (8) is assumed to occur both by diffusion and by convection.

The mass balance for VO^{2+} in the area between the surface of the particle and the bulk could be written, (using m as the $V^{(IV)}$ molar concentration), as following:

Dissolution flux₍₇₎ \approx dissociation flux₍₈₎ \approx diffusion flux₍₉₎ = accumulation of VO^{2+} flux into the bulk

$$\left(\frac{\partial m}{\partial t} \right)_{\text{bulk}} = S \times D \times (\text{grad } \bar{C})_{\text{surface of particle}} \quad (\text{Fick's 1st law}) \quad (5)$$

To simplify, the $VOSO_4 \cdot 5H_2O$ solid particles are considered spherical and a simple film model around the particle is creating the limitation to mass transfer (i.e. one direction transfer), the previous equation can be simplified as following:

$$\left(\frac{\partial m}{\partial t} \right)_{\text{bulk}} = S \times D \times \left(\frac{\partial \bar{C}}{\partial R} \right)_{\text{surface of particle}} \Rightarrow S \times k_{(t)} \times (C_{\text{sat}} - C_{\text{bulk}}) \quad (6)$$

The effect of the convection was examined on the mass transfer coefficient $k_{(t)}$, using the expression of Ranz and Marshall relative to a forced convection around a solid sphere (Cussler, 1984) (also known as the Leveque correlation providing the Sherwood number),

$$Sh \text{ Sherwood number} = \frac{k_{(t)} \times d_p}{D} = 2 + a \times Re^{1/2} \times Sc^{1/3} \quad (7)$$

This correlation is appropriated for spherical particles having the same size. In order to improve its applicability on the present case, some assumptions will be considered:

The calculations will be achieved assuming the presence of four separated size ranges of the solid particles having an initial radius $R^0 = 20, 40, 500$ and $1000 \mu\text{m}$ representing respectively 20%, 35%, 35% and 10% of the total solid volume (see curve of Fig. 2 1, cumulated volume);

All the particles of the powder will be assumed spherical, despite the various shapes observed (Fig. 1). Considering Eq. (7), the constant "a" is generally assumed equal to 0.6. However, in the present study and because of the large size distribution, "a" will be taken as an adjusting factor, which effect will be examined.

The molar quantity of the dissolved VO^{2+} "m" for N particles of initial radius R^0 can be expressed as:

$$m \frac{\rho \times V}{M} = N \times V_{\text{one particle}} \times \frac{\rho}{M}$$

$$N \times \frac{4}{3} \pi \times (R^3 - R_{(t)}^3) \times \frac{\rho}{M} \quad (8)$$

(Refer to notation and symbols)

The concentration of VO^{2+} in solution can be written as $C_{\text{bulk}} = \frac{m}{V_l}$; V_l being the total volume of the suspension (including both the liquid and the solid).

Combining Eqs. (6)–(8) leads to Eq. (9) describing the variation of the radius R of the solid particles as a function of time, and representing the dissolution rate \dot{R} of the vanadyl sulfate:

$$\dot{R} \Rightarrow \frac{dR}{dt} = \frac{A_1 A_2 (R^3 - R_{(t)}^3) + A_3 \sqrt{R_{(t)}} A_4 (R^3 - R_{(t)}^3) \sqrt{R_{(t)}}}{R_{(t)}} \quad (9)$$

where A_1 to A_4 are constants (refer to Appendix A for their developed expressions).

Eq. (9), written as $\dot{R} \Rightarrow \frac{dR}{dt} = f(R)$, is solved numerically using the Euler method ($R_{j+1} = R_j + \text{step} \times f(R, t)$) and enables to calculate a theoretical radius at time t , given that at $t^0 = 0$, $R = R^0$.

Note that the step used is: $\frac{\text{reaction time}}{\text{number of iterations}} = \frac{10}{100} = 0.1 \text{ min}$

The value of the radius R of a certain particle of $\text{VOSO}_4 \cdot 5\text{H}_2\text{O}$, obtained at a certain time t , from the resolution of Eq. (9) enables to obtain the theoretical values of the dissolved quantity of VO^{2+} i.e. the moles number, using Eq. (8).

Note that Eq. (9) is resolved 4 times, each for one of the chosen initial R^0 (20, 40, 500 and 1000 μm) of the solid particles and the total concentration of the dissolved vanadium sulfate (VO^{2+}) in solution is deduced (sum of the four obtained values of molar quantity divided by V_l). Also, for each R^0 , a different value of the adjusting factor “ a ” (Eq. (7)) was determined.

Fig. 6 shows two examples of the iterative determination, at 30 °C, of the optimal value of two parameters (the constant “ a ” in the Leveque equation and the percentage of each particle size range which directly affects the number of total particles N of each R^0). The optimized value of “ a ” or “ N ”, is the one leading to a curve of the concentration of the dissolved vanadium sulfate which fits best with the experimental data curve.

Following this iterative mode enables to evaluate the calculated curves at each temperature and the results are presented in Fig. 7 comparatively to the experimental data. Note that the viscosity was calculated for each temperature (Fassulo, 1965), while the value of the diffusivity at 25 °C (Jiang et al., 2016) was used for all the examined temperatures.

A relatively good agreement ($\frac{\Delta C}{C} \pm 0.1 \text{ M} / \sim 1.5 \text{ M}$) is observed between the results of the model and the experimental ones. Discrepancies are observed for short durations of the dissolution ($t < 1 \text{ min}$) because of the difficulty to standardize rapidly the suspension and to achieve precise measurement at the first few seconds after the stirring begins

Another difficulty comes from the dissolution of the smallest particles, which exhibit fast kinetics. In fact, compared to the bigger particles, this introduces additional uncertainties because the number of small particles of powder was not exactly taken into account.

To sum up, the obtained results lead to the following conclusions:

Regarding the effect of temperature:

- The initial dissolution rate increases with temperature.
- The solubility of the vanadyl sulfate at saturation (when the equilibrium of dissolution is reached) increases slightly with the temperature in the examined range of 5–30 °C, and this is compatible with the dissociation of an ionic salt weakly bonded.

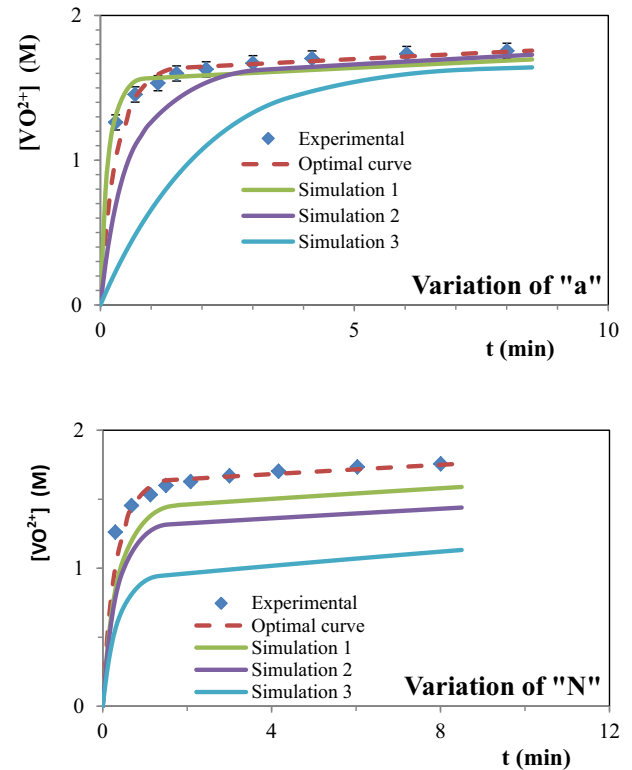


Fig. 6. Temporal evolution of the concentration of VO^{2+} released by the dissolution of the $\text{VOSO}_4 \cdot 5\text{H}_2\text{O}$ commercial powder: dots = experimental curves; Continuous lines = simulated curves obtained with the non optimized parameter value, i.e. the constant “ a ” in the Leveque equation (figure on the top), and the percentage of each particle size range which directly affects the number of total particles “ N ” of each R^0 (figure on the bottom); Broken lines = simulated curves obtained with the optimized parameters of “ a ” (figure on the top), and “ N ” (figure on the bottom).

Both the stirring of the suspension and the size of the particles strongly affect the dissolution rate (mainly for dissolution times lower than 5 min), proving that the dissolution kinetics of the vanadyl sulfate (to VO^{2+}), is limited by the mass transfer of VO^{2+} from the solid powder surface to the bulk, while the chemical reaction with the proton is not limiting.

3.2. Dissolution of vanadium pentoxide

3.2.1. Characterization of the initial powder

The commercial powder of V_2O_5 was characterized by SEM and laser diffraction particle sizing technique. The SEM micrograph in Fig. 8 1 shows that the V_2O_5 particles form agglomerated sticks of various sizes. The size distribution (Fig. 8 2) shows a large dispersion of particle size from 120 nm to 4 μm .

The graph exhibits three peaks located respectively at 2, 80 and 900 μm ; therefore, in order to study the effect of particles size on the dissolution kinetic, the initial powder was sieved using four different cut off threshold sieves: 315 μm ; 200 μm ; 120 μm and 80 μm . Thus, five different diameter ranges of powder were obtained: $d_p > 315 \mu\text{m}$; $315 > d_p (\mu\text{m}) > 200$; $200 > d_p (\mu\text{m}) > 120$; $120 > d_p (\mu\text{m}) > 80$ and $d_p (\mu\text{m}) < 80$, three of which were used to carry out dissolution experiments.

3.2.2. Effect of temperature on dissolution kinetics

The effect of temperature on the dissolution of vanadium pentoxide was studied in the range 0–40 °C and the temporal evolution of the dissolved VO_2^+ concentration is presented in Fig. 9.

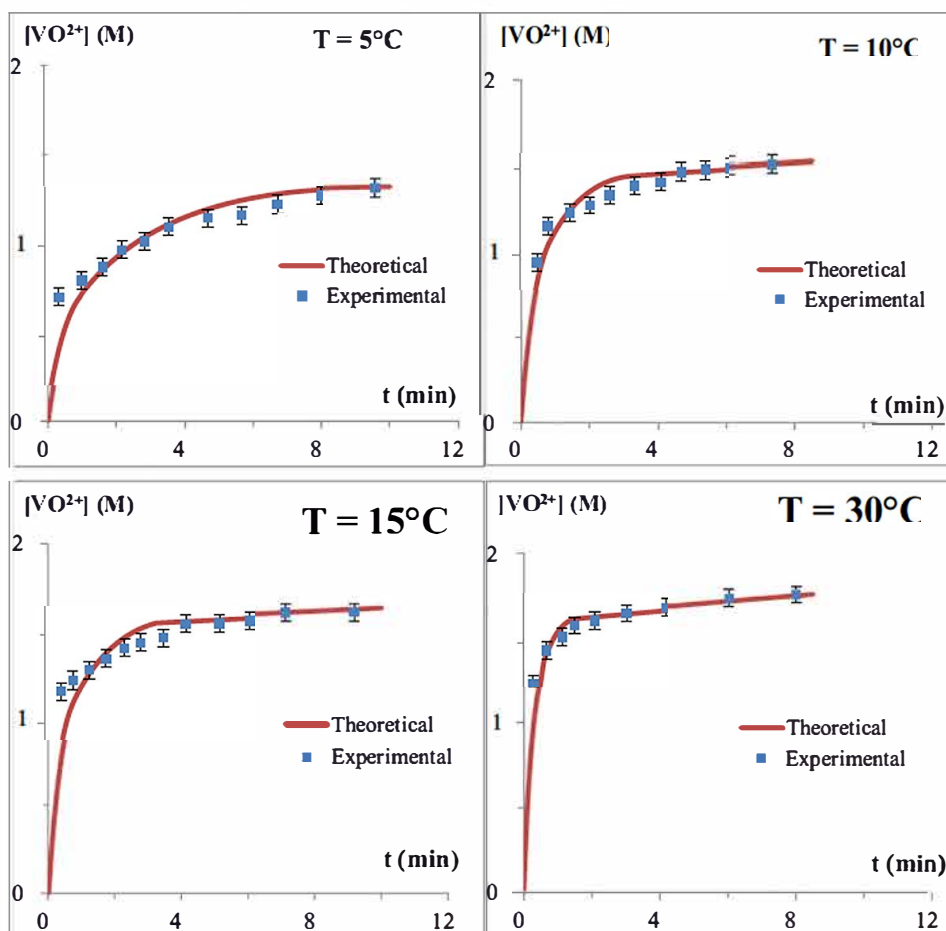


Fig. 7. Comparison between the experimental data (reported from Fig. 3) and the model (calculated using Eq. (9)) of the temporal evolution of the concentration of VO_2^+ released by the dissolution of a $\text{VOSO}_4 \cdot 5\text{H}_2\text{O}$ commercial powder, at various temperatures.

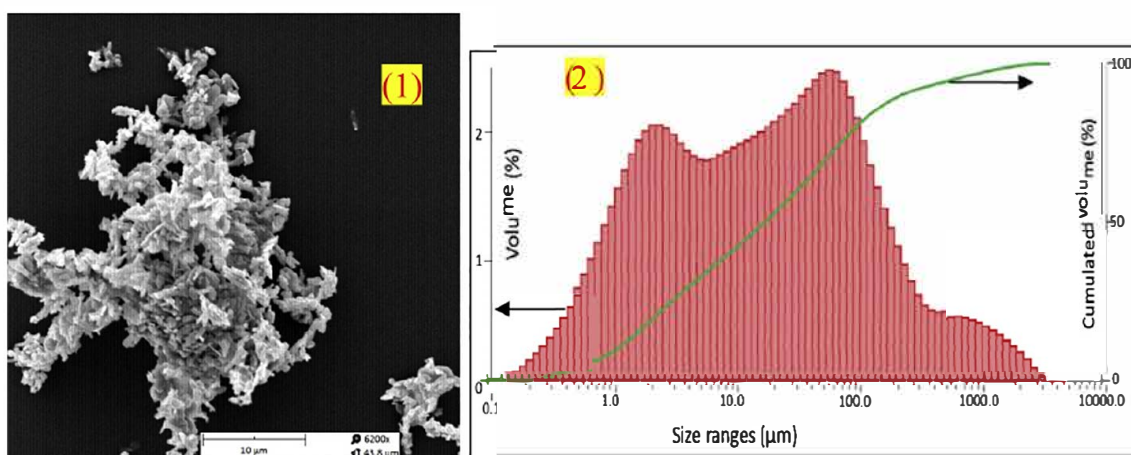


Fig. 8. (1) SEM pictures (10 kV-Point, SED) and (2) size distribution obtained (by laser diffraction sizing technique: P = 3 bar, dry mode) of the vanadium pentoxide V_2O_5 commercial powder.

The behavior is rather similar for each temperature: a rapid dissolution occurs at "short" reaction times (less than 1 h) and then the concentration tends to reach a constant value. Note that, for all the examined temperatures (except 0 °C), the dissolution equilibria of the vanadium pentoxide to VO_2^+ is achieved after 5 h of

stirring; for the dissolution at 0 °C a higher reaction time is required to reach the saturation.

Several differences can be observed compared to the dissolution features of VOSO_4 :

The saturation concentrations (C_{sat}) of VO_2^+ are about three times lower than those of the VO_2^{2+} ; in addition, the C_{sat} decreases when the temperature increases (contrary to the case of the $V^{(IV)}$, where C_{sat} increases with T). This point will be analyzed in the next section.

For the stronger stirring (500 rpm), the time required to dissolve the oxide and to reach the saturation concentration of VO_2^+ is more than fifty times higher than that required for the VO_2^{2+} . Typical comparative values are 5 min to reach a concentration of VO_2^{2+} of 1.5 M, while 3 h were required to reach a concentration of VO_2^+ of 0.5 M. Moreover, at 40 °C, the saturation concentration of VO_2^+ is reached for $t < 20$ min, while at 0 °C the solution is not saturated, even after 5 h. Another experiment was carried out at 0 °C where the suspension of vanadium pentoxide was left under stirring for one day. The concentration of the dissolved VO_2^+ was determined and the following values were obtained: $[VO_2^+]_{23h} = 0.788$ M and $[VO_2^+]_{25h} = 0.783$ M. This last result tends to show that the mass transport is not the limiting step.

The concentration of the VO_2^+ measured for reaction times lower than five minutes (named $t_{initial}$), will be used to estimate approximately the initial rate of the V_2O_5 dissolution r^0 (defined as the ratio $\frac{[VO_2^+]_{t_{initial}}}{t_{initial}}$).

Assuming, as for the vanadyl sulfate, that (i) the kinetic constant of the initial dissolution rate follows the Arrhenius law, and (ii) the others terms of the expression of the dissolution rate are independent of the temperature, then, the logarithmic analysis of the evolution of the initial rate with the temperature leads to the following correlation:

$$\ln r^0_{(r^0 \text{ in } \frac{M}{h})} = 22.7 \frac{8727.3}{T_{(in \text{ } K)}} \quad (10)$$

The slope of this linear relation enables the determination of a roughly estimated value of the activation energy of the dissolution process: $E_a = 73$ kJ/mol.

This energy is more than four times higher than the value obtained for the dissolution of $VOSO_4$ (18.8 kJ/mol). This could be explained by the fact that the hydration of the vanadium pentoxide (V_2O_5 which exhibits covalent bonds) followed by its reaction with H^+ ions is energetically more difficult to achieve, comparatively to the simple dissociation of the ionic salt $VOSO_4$.

3.2.3. Effect of available surface area on dissolution kinetics

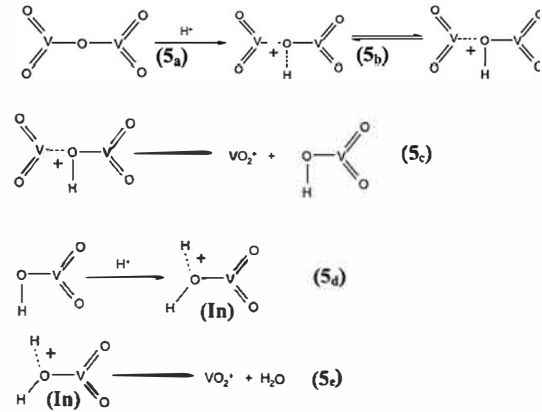
The effect of the particle size on the dissolution rate of V_2O_5 was examined at 40 °C and 500 rpm stirring rate and the results are shown in Fig. 10.

Practically the same concentrations were measured for the three different size ranges of the solid particles ($80 < d_p < 120 \mu m$, $120 < d_p < 200 \mu m$ and $200 < d_p < 315 \mu m$). These results tend to show that the dissolution rate does not depend on the solid/liquid exchange surface. Theoretically, the particle size affects the initial rate of the dissolution that should increase. However, in our case, owing to the low values of these dissolution rates, the curves do not have enough resolution to show any difference. Moreover, these results support our previous conclusion: the mass transfer does not represent a limitation to the dissolution of V_2O_5 but it is rather the chemistry of the system.

Consequently, the effect of stirring on the dissolution was not studied.

Since the dissolution is not significantly affected by the particles size, the possibility of kinetic control by surface passivation was evaluated.

A simplified reaction scheme is proposed below for the vanadium pentoxide dissolution (R5):



Hydrogen ion attacks the oxide and the product obtained from reaction (5b) decomposes according to reaction (5c); then by reaction with H^+ , it forms an intermediate (In) which dehydrates to lead to VO_2^+ .

However, another reaction pursue of the intermediate (In) could be its polymerization according to various reactions and in the last case, the external surface of each solid particle could be entirely covered by a passive layer that prevents the dissolution and could be the reason for which the observed saturation concentration of VO_2^+ remains low.

To clarify this point, the following dissolution experiment was carried out: a solid liquid suspension of the commercial V_2O_5 sieved powder ($200 < d_p < 315 \mu m$) was introduced into a H_2SO_4 3 M solution at 25 °C and stirred during 5 h. The results are illustrated in Fig. 11: the $[VO_2^+]$ increases to reach the saturation concentration (~ 0.55 M after $t \sim 1$ h) then remains constant. Then the suspension was filtered to remove the residual solid and a fresh sample of the powder was added into the filtrate. The dissolution experiment was pursued for 6 h, and the temporal evolution of the concentration of the vanadium is indicated into Fig. 11 (for $t > 22$ h until $t = 28$ h). The renewal of the solid does not change the dissolved amount of vanadium, implying that the equilibrium was reached and no further dissolution can be achieved. This test confirms that there is no passivating or inhibiting layer formed on the surface of the particles.

3.2.4. Equilibrium data

The saturation concentration of VO_2^+ , obtained for $t > 5$ h (extracted from Fig. 9), are reported in Fig. 12, simultaneously with the values from Rahman (1998), Skyllas Kazacos et al. (2016). Note that the values extracted from the bibliography were multiplied by 2 in order to obtain the concentration of VO_2^+ , instead of the solubility of V_2O_5 used in the cited references. The saturation concentration of VO_2^+ decreases when the applied temperature increases, even if a shorter time is required to reach the equilibrium.

The equilibrium constant of reaction (5) can be written as a function of the activities of the species in solution:

$$K_{(5)} = \frac{(a_{VO_2^+})^2 \times a_{H_2O}}{a_{V_2O_5 \text{ solid}} \times (a_{H^+})^2} = \frac{a_{H_2O} \times (\gamma_{VO_2^+})^2}{a_{V_2O_5 \text{ solid}} \times (\gamma_{H^+})^2} \times \left(\frac{[VO_2^+]}{[H^+]^0} \right)^2 \quad (11)$$

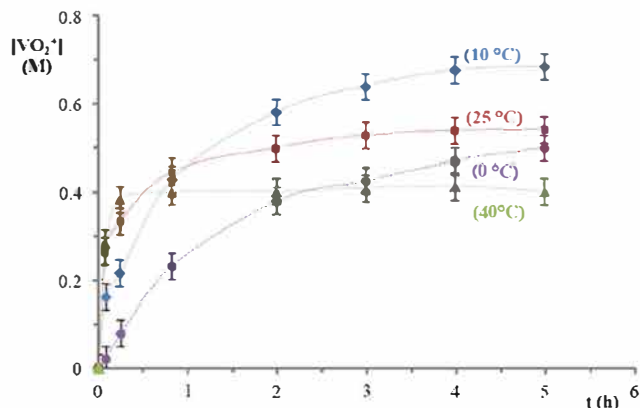


Fig. 9. Temporal evolutions of the concentration of the VO_2^+ (released by the dissolution of a V_2O_5 commercial powder), at various temperatures; $[\text{H}_2\text{SO}_4] = 3 \text{ M}$; stirring 500 rpm.

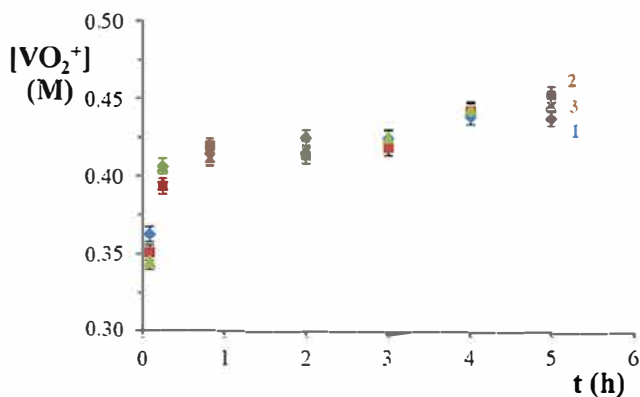


Fig. 10. Temporal evolutions of the dissolved VO_2^+ concentration (released by the dissolution of a V_2O_5 commercial powder) for various initial sizes of the solid particles of V_2O_5 obtained by sieving; $[\text{H}_2\text{SO}_4] = 3 \text{ M}$, stirring 500 rpm, sieved V_2O_5 powder, $T = 40 \text{ }^\circ\text{C}$. (1) $80 < d_p < 120 \text{ } \mu\text{m}$; (2) $120 < d_p < 200 \text{ } \mu\text{m}$; (3) $200 < d_p < 315 \text{ } \mu\text{m}$.

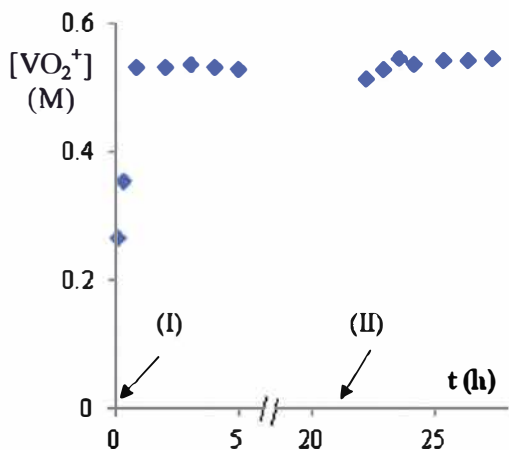


Fig. 11. Temporal evolution of the VO_2^+ concentration (released by the dissolution of a V_2O_5 commercial powder) for two different additions of solid samples of V_2O_5 into the liquid; 15 cm^3 of $[\text{H}_2\text{SO}_4] = 3 \text{ M}$, stirring 500 rpm, $T = 25 \text{ }^\circ\text{C}$, sieved V_2O_5 powder ($200 < d_p < 315 \text{ } \mu\text{m}$). (I) first introduction of 2.2 g of V_2O_5 ; (II) filtration and second introduction of 2.2 g of V_2O_5 .

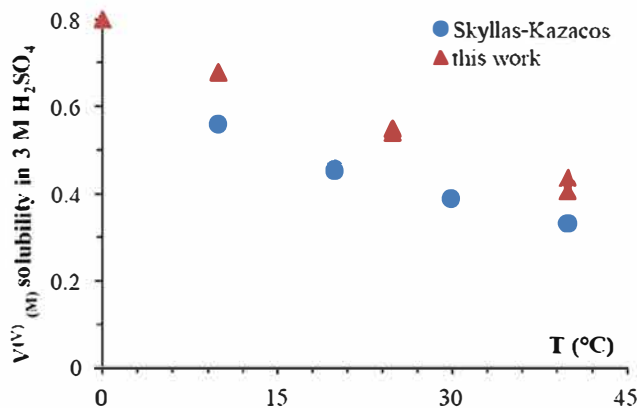


Fig. 12. Influence of temperature on the solubility of $\text{V}(\text{V})$. Triangles: this work; circles: Rahman (1998), Skyllas-Kazacos et al. (2016).

In the present case, the concentrations of the VO_2^+ at saturation are lower than the values obtained for VO^{2+} at saturation (Fig. 9: 0.4–0.7 M for stirring duration of 5 h). The effect of the concentration on the activity coefficient will also be examined in a future work via the Pitzer model.

For the time being, in order to get a preliminary rough estimation of the sensitivity of the vanadium pentoxide solubility against

the temperature, the term $\frac{a_{\text{H}_2\text{O}} \times (\gamma_{\text{VO}_2^+})^2}{a_{\text{V}_2\text{O}_5 \text{ solid}} \times (\gamma_{\text{H}^+})^2}$ will be considered constant and named ξ . Then a logarithmic analysis of the data at the equilibrium (Fig. 9) versus the reverse temperature was performed according to the following equation:

$$\ln \left(\frac{[\text{VO}_2^+]_{\text{sat}}}{[\text{H}^+]^0 [\text{VO}_2^+]_{\text{sat}}} \right) = 0.5 \times (\text{constant} \ln \xi) \frac{k'}{2R} \times \frac{1}{T} \quad (12)$$

The linear regression analysis of the experimental results leads to the following equation $\ln \left(\frac{[\text{VO}_2^+]_{\text{sat}}}{[\text{H}^+]^0 [\text{VO}_2^+]_{\text{sat}}} \right) = 9.15 + \frac{2272}{T}$ with a correlation coefficient with the experimental results of $R^2 = 0.9997$, a satisfactory value taking into account the uncertainties on the dependence of the activity coefficient to the concentration.

The slope of the above equation ($+2272 \text{ k}'/(2R)$), enables to deduce $k' = -37.8 \text{ kJ/mol}$, a negative value; it could be attributed, very approximately, to the changes in the enthalpy of the reaction between H^+ and V_2O_5 which appears to be an exothermic process. This is also confirmed by the bibliography and particularly the studies of (Rahman and Skyllas Kazacos, 2009) which claims that the reaction (5) is an endothermic reaction. Note that, the obtained negative value is in agreement with the effect of temperature on the saturation concentration: the saturation concentration of VO_2^+ decreases when the temperature of the stirred suspension increases.

Besides comparison of k for the vanadyl sulfate ($+16.3 \text{ kJ/mol}$) and k' for the vanadium pentoxide (-37.8 kJ/mol) enables to conclude that the dissolution of both vanadium compounds follows different schemes: the process is endothermic for the dissolution of VOSO_4 and exothermic and more 'difficult' for the breaking of the oxide bonds ($\text{V}-\text{O}$ bond have a more covalent character than bond $\text{VO}-\text{SO}_4$ bond).

3.2.5. Kinetic model of the dissolution

The comparison of the dissolution of both VOSO_4 and V_2O_5 lead to the following conclusions:

The time required to saturate the solution with VO_2^+ is in the order of "some hours" compared to a time in the order of some minutes for VO^{2+} , especially for 'low' temperature (0°C). Moreover, the saturation concentration of the VO_2^+ is, as function of T , much lower than the saturation concentration of VO^{2+} ; Taking into account the fact that 5 h were required to saturate the $\text{V}^{(V)}$ solution, it can be concluded that the mass transfer is not a limiting factor of the oxide dissolution. Besides, it was shown that the observed limitation in the V_2O_5 dissolution does not come from the physical properties of the powder, nor from an eventual secondary reaction taking place on the particles' surface and blocking the main dissolution (§ 3.2.3).

Therefore, the dissolution of the $\text{V}^{(V)}$ will be assumed to be limited by the chemistry of the reaction (5) assumed to be a slow equilibrium, of which the global rate can be expressed by the Eq. (13).



$$r_{(5)} = \frac{1}{2} \frac{d[\text{VO}_2^+]}{dt} = k_{f(5)} \times \left(\frac{N_{\sigma_i}}{N_a}\right)^\alpha \times \left(\frac{\text{moles of H}^+}{V_{\text{suspension}}}\right)^\beta \times \left(\frac{\text{moles of VO}_2^+}{V_{\text{suspension}}}\right)^\gamma \quad (13)$$

(Refer to Appendix B for the detailed development of Eq. (13))
Thus, for particles 'i' having, at the time t:

S_i as surface
 N_{σ_i} sites on their surface, and
releasing by dissolution $2(X)_{S_i}$ moles of VO_2^+

The dissolution rate Eq. (13) can be expressed as following:

$$r_{(5)S_i} = \frac{1}{2} \frac{d[\text{VO}_2^+]_{S_i}}{dt} = \frac{1}{2} \frac{d(2X)_{S_i}}{V_{\text{suspension}} dt} = \frac{d(X)_{S_i}}{V_{\text{suspension}} dt} = k_{f(5)} \times \left(\frac{N_{\sigma_i}}{N_a}\right)^\alpha \times \frac{\left\{n^{\circ\text{H}} \cdot 2 \times (X)_{S_i}\right\}^\beta}{V_{\text{suspension}}^\beta} \times k_{r(5)} \frac{\left\{2 \times (X)_{S_i}\right\}^\gamma}{V_{\text{suspension}}^\gamma} \quad (14)$$

The same equation will be written three times, because for the calculation, three particle surfaces S_1 , S_2 and S_3 are considered relatively to three particle diameters: 10, 60 and 1000 μm according to the Fig. 8 2.

Then the resolution of each equation will provide the released moles number $(2X)_{S_i}$ of VO_2^+ , and in order to determine the global released moles number of VO_2^+ , it is necessary to sum the four individual moles numbers, i.e. $(2X)_{\text{global}} = (2X)_{S_1} + (2X)_{S_2} + (2X)_{S_3}$.

On the other hand, the expression of N_{σ} , considered to be the number of available V_2O_5 sites, as a function of the particle radius R_i and the vanadium initial concentration can be written as:

$$N_{\sigma_i} = \frac{N_i}{\sigma^\circ} \times \left(\frac{3(4\pi)^{0.5} M}{\rho}\right)^{2/3} \times (n^{\circ\text{V}} \cdot X_{R_i})^{2/3}$$

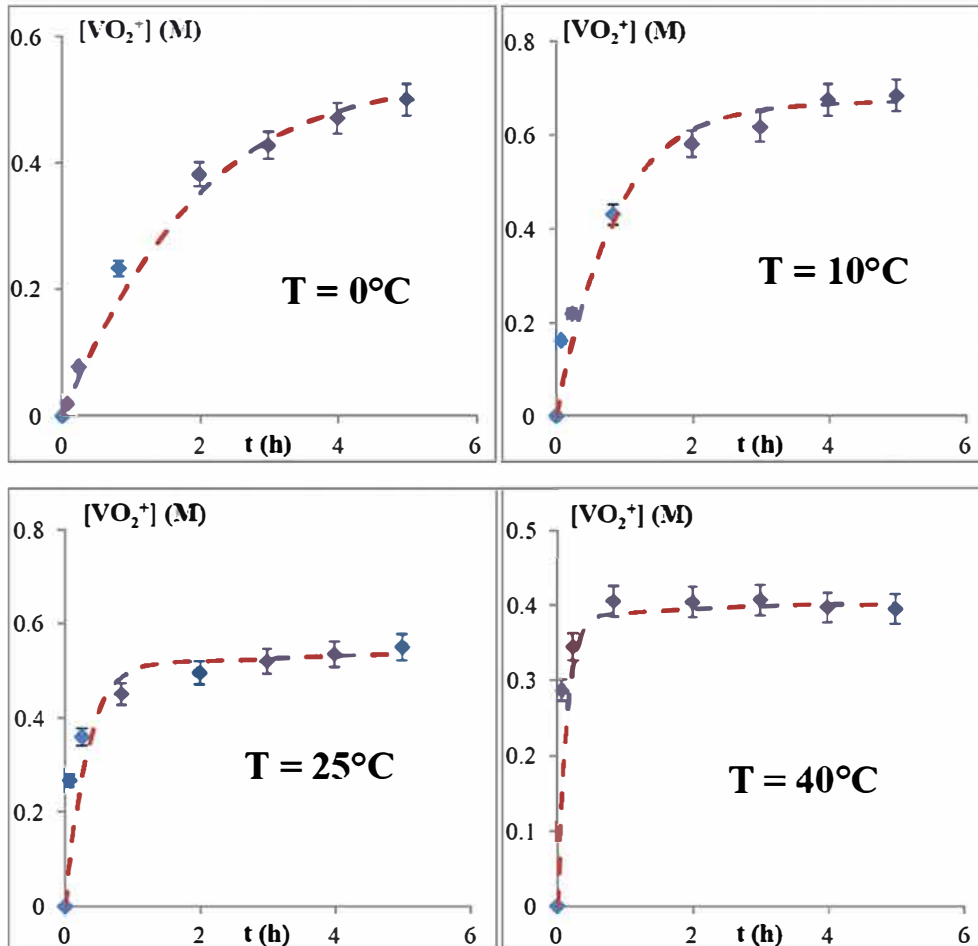


Fig. 13. Comparison between the experimental data (diamonds, imported from Fig. 9) and the model (broken lines, calculated using Eq. (15)) for the temporal evolution of the concentration of VO_2^+ released by the dissolution of a V_2O_5 commercial powder, at various temperatures.

Table 1

Iteratively estimated values of the kinetic constants $k_{(5)}$ and $k_{(-5)}$ for the studied temperatures, and their corresponding activation energies (estimations).

Temperature (°C)	$k_{(5)}$ (mol ⁻² s ⁻¹ L g)	$k_{(-5)}$ (mol ⁻¹ s ⁻¹ L)
0	0.9×10^{-4}	2.3×10^{-4}
10	2.6×10^{-4}	3.4×10^{-4}
25	4.8×10^{-4}	13×10^{-4}
40	7×10^{-4}	41×10^{-4}
Activation energy (estimated by $k = Ae^{E_a/RT}$)	E_a (5) = 34.5 kJ/mol	E_a (-5) = 52.9 kJ/mol

Substituting it in Eq. (14) and considering the reaction orders with respect to V_2O_5 , H^+ and VO_2^+ , to be equal to their stoichiometric coefficients, the expression of global rate of the reaction is:

$$r_{(5)S_i} = \frac{d(X)_{S_i}}{dt} = k_{(5)} \times \frac{N_i}{N_a \times \sigma^\circ} \times \left(\frac{3(4\pi)^{0.5} M}{\rho} \right)^{2/3} \times (n^{\circ} V_{R_i})^{2/3} \times \frac{\left\{ n^{\circ} H \right\}^2 \times \left\{ 2 \times (X)_{S_i} \right\}^2}{V_{suspension}} \times k_{(-5)} \frac{\left\{ 2 \times (X)_{S_i} \right\}^2}{V_{suspension}} \quad (15)$$

Eq. (15), solved numerically using the Euler method, provides the variation of the quantity of VO_2^+ as a function of time. The only unknown parameters are $k_{(5)}$ and $k_{(-5)}$, the kinetic constants of the forward and backward reaction. They will be adjusted in order to determine the theoretical evolution of the VO_2^+ concentration which correctly correlates with the experimental one.

Fig. 13 shows the correlation between the calculated values of dissolved VO_2^+ (broken lines) and the experimental data (diamonds). The values of the kinetic constants, enabling to get a satisfactory agreement between theory and experiment, are indicated in Table 1.

The results show that the backward kinetic constant $k_{(-5)}$ is more sensitive to the temperature than the forward $k_{(5)}$. Besides, for all the examined temperatures, $k_{(-5)}$ is higher than the $k_{(5)}$. This means that the dissolution of the oxide is allowed only for 'relatively' low concentrations of VO_2^+ , enabling to keep the term of the backward rate lower than this of the forward rate.

Note also that, because the order against the H^+ concentration (in the forward term of the rate) is equal to 2, the acidic media is beneficial to the dissolution of the oxide and this is also in agreement with the results of Rahman and Skyllas Kazacos (2009).

4. Conclusion

Numerous works exist in the field of the vanadium battery and one important objective is to avoid the vanadium pentoxide precipitation, because its dissolution seems difficult. In addition, the published studies do not exhibit the determination of the physical limitations and phenomena to be overcome, in order to act upstream. The aim of present work was the study of the dissolution mechanisms of the vanadyl sulfate $VOSO_4$ and vanadium pentoxide V_2O_5 in 3 M sulfuric acid, under various operative conditions, and also to bring knowledge on the understanding of the phenomena governing these dissolutions.

Several experimental data giving the temporal evolution of the dissolved vanadium concentrations versus various operating parameters were acquired and supplied. Moreover, kinetic laws describing both dissolution limitations phenomena were determined and explained. As expected these compounds exhibit different behaviors towards dissolution. The general results show that the dissolution of $VOSO_4 \cdot 5H_2O$, an 'ionic salt', appears to be easier

and more rapid, comparatively to that of the V_2O_5 oxide (which is covalently bonded).

Their initial dissolution rate increases with temperature, for both compounds $VOSO_4$ and V_2O_5 , and the rough estimations of the activation energies at the beginning of the dissolution (18.8 kJ/mol for $VOSO_4$ and 73 kJ/mol for V_2O_5) clearly show that the temperature influence two different phenomena: the mass transport for the vanadyl sulfate, and the reaction with the proton for the vanadium pentoxide.

The saturation concentration of the VO^{2+} is reached after few minutes of stirring (<10 min), while several hours (>5h) were required for the VO_2^+ released by the oxide V_2O_5 to reach saturation (and more than 1 day at 0 °C). In addition the solubility of the $V^{(IV)}$ salt is higher than the solubility of the oxide (at least two times, even three for certain temperatures): VO^{2+} concentrations of 2 M can be achieved from the dissolution of $VOSO_4$ at $T \geq 30$ °C, while for the oxide dissolution the VO_2^+ saturation concentration reaches ~0.45 M at 40 °C.

Moreover, conversely to the $V^{(IV)}$, in the case of vanadium pentoxide decreasing the temperature causes the saturation concentration of VO_2^+ to increase: from 0.42 to 0.78 M respectively at 40 and 0 °C, and the whole dissolution process appears to be exothermic ($k' = 37.8$ kJ/mol).

Concerning the kinetic models, the dissolution of $VOSO_4$ consists of the dissociation in the acid media, followed by its dispersion in the bulk. The whole process is limited by mass transport (more specifically diffusion and convection). The accumulation flux of VO^{2+} was expressed using Fick's 1st law and the Sherwood correlation and the simulated results enable to reproduce experimental measurements and to validate the mass transport limitation. For V_2O_5 , the dissolution rate appears to be limited by a chemical reaction (acidic attack followed by the breaking bonds). A simple reaction scheme was proposed for the dissolution and its rate was expressed assuming the chemical reaction as an elementary reaction. The model agrees with the experimental data and the resulting kinetic constants show a backward reaction (-5) more sensitive to temperature and having a rate in certain conditions higher than the rate of the forward reaction (5).

Note that the obtained results were very sensitive to the sulfuric acid concentration which changes during the battery operation (increases during the charge and decreases during the discharge). The 3 M of sulfuric acid was chosen as a compromise between its positive effect on the dissolution of the vanadium pentoxide and its negative effect on the dissolution of vanadium sulfate.

To sum up, in the absence of chemical additives enabling to keep the $V^{(V)}$ under dissolved form and avoid precipitation of the vanadium pentoxide, it is required to operate in strong acidic conditions, with a "discharged battery" instead of a "battery completely charged". Moreover, a charged vanadium battery will exhibit a more stable behavior if stored in low ($T < 20$ °C) temperature conditions, rather than in high temperature conditions ($T > 40$ °C). Also, taking into account the results of the bibliography, it is better to avoid maintaining the battery in recharged state for a long time.

Declaration of interests

The authors declare that there is no conflict of interest.

Acknowledgments

This study was supported by the Agence Nationale de la Recherche, France. The authors would like to acknowledge Brigitte Dustou, Laure Latapie and Sandrine Desclaux for the technical support they provided for the accomplishment of this work.

Appendix A

The combination of Eqs. (6)–(8) enables to obtain the expression of $\frac{dR}{dt}$ (Eq. (9)) also noted \dot{R} expressing the variation of the particles radius over time and representing the dissolution rate of the $V_2O_5 \cdot 5H_2O$. To reach this expression, the following calculation steps were followed:

$$Sh \frac{k(t) \times d_e}{D} \left(2 + a \times Re^{\frac{1}{2}} \times Sc^{\frac{1}{3}} \right) \rightarrow k(t) \frac{D}{2R} \left(2 + a \times Re^{\frac{1}{2}} \times Sc^{\frac{1}{3}} \right)$$

$$\left(\frac{dm}{dt} \right)_{R \rightarrow \infty} + S \times k(t) \times (C_{sat} - C_{bulk})$$

$$\frac{d \left(\frac{4}{3} \pi \times \frac{\rho \times N}{M} \times (R^{o3} - R^3) \right)}{dt} = 4\pi R^2 \times \left(\frac{D}{2R} \left(2 + a \times Re^{\frac{1}{2}} \times Sc^{\frac{1}{3}} \right) \times \right.$$

$$\left. (C_{sat} - \frac{4}{3} \pi \times \frac{\rho \times N}{M \times V_l} \times (R^{o3} - R^3)) \right)$$

Developing the above equation leads to:

$$\frac{R \times dR}{dt} = \frac{MDC_{sat}}{\rho} - \frac{4}{3} \pi \frac{ND}{\rho V_l} (R^{o3} - R^3) + \frac{aMC_{sat}}{2\rho} (2 \omega)^{\frac{1}{2}} D^{\frac{2}{3}} \nu^{(-\frac{1}{6})} R^{\frac{1}{2}}$$

$$- \frac{4}{6} \pi \frac{aN}{V_l} (2 \omega)^{\frac{1}{2}} D^{\frac{2}{3}} \nu^{(-\frac{1}{6})} (R^{o3} - R^3) R^{\frac{1}{2}}$$

$$\dot{R} \Rightarrow \frac{dR}{dt} = \frac{A_1 - A_2 (R^{o3} - R^3) + A_3 \sqrt{R} - A_4 (R^{o3} - R^3) \sqrt{R}}{R} \quad (9)$$

A_1	A_2	A_3	A_4
$\frac{M \times D \times C_{sat}}{\rho}$	$\frac{4}{3} \pi \frac{D \times N}{V_l}$	$\frac{aMC_{sat}}{2\rho} (2 \omega)^{\frac{1}{2}} D^{\frac{2}{3}} \nu^{(-\frac{1}{6})}$	$\frac{4}{6} \pi \frac{aN}{V_l} (2 \omega)^{\frac{1}{2}} D^{\frac{2}{3}} \nu^{(-\frac{1}{6})}$

Appendix B

$$r_{(5)} = \frac{1}{2} \frac{d[VO_2^+]}{dt} \times k_{(5)} \times \left(\frac{N_{\sigma}}{N_a} \right)^{\alpha} \times \left(\frac{\text{moles of } H^+}{V_{suspension}} \right)^{\beta} \times k_{(5)} \times \left(\frac{\text{moles of } VO_2^+}{V_{suspension}} \right)^{\gamma} \quad (13)$$

The following nomenclature will be used to treat this equation and to determine the theoretical concentration of VO_2^+ :

For the considered weight of the V_2O_5 particles having as initial diameter: 10, 60 and 1000 μm (from Fig. 8), it will be noted:

$S_1^o, S_2^o, \text{ and } S_3^o$: their average initial surface.

$S_1, S_2 \text{ and } S_3$: their average surface at the time t.

$R_1^o, R_2^o \text{ and } R_3^o$: their average initial radii.

$R_1, R_2 \text{ and } R_3$: their average radii at the time t.

also:

$N_1, N_2 \text{ and } N_3$: are the number of particles having as initial diameter: 10, 60 and 1000 μm

$N_{\sigma 1}, N_{\sigma 2} \text{ and } N_{\sigma 3}$: are the number of sites (i.e. the number of the V_2O_5 molecules) accessible to the proton H^+ , at time t for the particles having as initial diameter: 10, 60 and 1000 μm

σ^o : is the surface occupied by one molecule of V_2O_5

N_a : Avogadro number

the exponents α, β and γ are the reaction orders, respectively for a site constituted by V_2O_5, H^+ and VO_2^+ ;

$k_{(5)}$ and $k_{(5)}$ the forward and backward kinetic constants respectively.

N_{σ} = the number of sites accessible to H^+ , at time t
 $= N_{\sigma 1} + N_{\sigma 2} + N_{\sigma 3} \frac{\text{surface of the particles at the time } t}{\text{surface occupied by one molecule}} \frac{\Sigma(N_j \times S_j)}{\sigma^o}$

in addition: " n_V ", and " n_H " represents respectively the initial moles number of V_2O_5 and H^+ ,

"X" the moles number of V_2O_5 dissolved at time t, by consumption of $2X$ moles of

H^+ , and releasing $2X$ moles of VO_2^+ ;

$$r_{(5)S_i} = \frac{1}{2} \frac{d[VO_2^+]}{dt} \times \frac{1}{2} \frac{d(2X)_{S_i}}{V_{suspension} dt} \times \frac{d(X)_{S_i}}{V_{suspension} dt} \times k_{(5)} \times \left(\frac{N_{\sigma i}}{N_a} \right)^{\alpha} \times \frac{\{n_H - 2(X)_{S_i}\}^{\beta}}{V_{suspension}^{\beta}} \times k_{(5)} \times \frac{\{2 \times (X)_{S_i}\}^{\gamma}}{V_{suspension}^{\gamma}} \quad (14)$$

Moreover, the following changes are required in order to transform Eq. (14) into a resolvable form:

$$N_{\sigma i} \frac{S_i}{\sigma^o} = \frac{4\pi \times N_i}{\sigma^o} R_i^2 \quad (A)$$

Besides the mass of the V_2O_5 introduced into the suspension is: $m_{V_2O_5} = m_{R_1} + m_{R_2} + m_{R_3}$

The mass of V_2O_5 particles having R_i as diameter can be expressed by the two following equations:

m_{R_i} Molecular weight of $V_2O_5 \times$ mol number of particles having R_i $M \times n_{VR_i}$

$$\text{and } m_{R_i} = \rho V_{solide R_i} = \rho \frac{4\pi R_i^3}{3}$$

Combining both equations leads to: $M \times n_{VR_i} = \rho \frac{4\pi R_i^3}{3} \Rightarrow$

$$R_i = \left\{ \frac{3Mn_{VR_i}}{4\pi\rho} \right\}^{\frac{1}{3}} \quad (B)$$

Substituting (B) into (A) gives the number of sites having, at time t, R_i as initial diameter:

$$N_{\sigma i} = \frac{4\pi \times N_i}{\sigma^o} \left(\left\{ \frac{3Mn_{VR_i}}{4\pi\rho} \right\}^{\frac{1}{3}} \right)^2 \Rightarrow N_{\sigma i} = \frac{N_i}{\sigma^o} \times \left(\frac{3(4\pi)^{0.5} Mn_{VR_i}}{\rho} \right)^{2/3}$$

And substituting n_{VR_i} by $(n^o_V - X_{R_i})$ gives \Rightarrow

$$N_{\sigma i} = \frac{N_i}{\sigma^o} \times \left(\frac{3(4\pi)^{0.5} M}{\rho} \right)^{2/3} \times (n^o_V - X_{R_i})^{2/3} \quad (C)$$

Substituting (C) into the expression of the rate (Eq. (14)) leads to:

$$r_{(5)S_i} = \frac{d(X)_{S_i}}{V_{suspension} dt} \times k_{(5)} \times \left(\frac{N_i}{N_a \times \sigma^o} \times \left(\frac{3(4\pi)^{0.5} M}{\rho} \right)^{2/3} \times (n^o_V - X_{R_i})^{2/3} \right)^{\alpha} \times \frac{\{n_H - 2(X)_{S_i}\}^{\beta}}{V_{suspension}^{\beta}} \times k_{(5)} \times \frac{\{2(X)_{S_i}\}^{\gamma}}{V_{suspension}^{\gamma}}$$

$$r_{(5)S_i} = \frac{d(X)_{S_i}}{dt} \times k_{(5)} \left(\frac{N_i}{N_a \times \sigma^o} \times \left(\frac{3(4\pi)^{0.5} M}{\rho} \right)^{2/3} \right)^{\alpha} \times \left((n^o_V - X_{R_i})^{2/3} \right)^{\alpha} \times \frac{\{n_H - 2 \times (X)_{S_i}\}^{\beta}}{V_{suspension}^{\beta}} \times k_{(5)} \times \frac{\{2 \times (X)_{S_i}\}^{\gamma}}{V_{suspension}^{\gamma}}$$

The size of all these equations appears to be so high!! why??? To solve this equation, the reaction orders are required and they will be assumed to be equal to the stoichiometric coefficients of each reactant, i.e. $\alpha = 1$ and $\beta = \gamma = 2$.

$$r_{(5)S_i} \frac{d(X)_{S_i}}{dt} = k_{(5)} \times \frac{N_i}{N_a \times \sigma^\circ} \times \left(\frac{3(4\pi)^{0.5} M}{\rho} \right)^{2/3} \times (n^\circ_v X_{R_i})^{2/3} \times \frac{\{n^\circ_H \quad 2 \times (X)_{S_i}\}^2}{V_{suspension}} \quad k_{(5)} \frac{\{2 \times (X)_{S_i}\}^2}{V_{suspension}} \quad (15)$$

Note that three equations must be solved for the three particle sizes chosen, each one providing the mole number of VO_2^+ produced by the dissolution of the corresponding family of these particles as indicated in the following table.

	$r_{(5)S_1}$	$r_{(5)S_2}$	$r_{(5)S_3}$
Dissolution rate relative to the particles having, at time t, an average Radii R_i (i going from 1 to 3, as defined above)	N_1	N_2	N_3
the number of the particles having, at time t, an average Radii R_i	$2X_{R_1}$	$2X_{R_2}$	$2X_{R_3}$
The mole number of VO_2^+ produced by the dissolution of the particles having, at time t, an average Radii R_i	Total mole number of VO_2^+ produced by the dissolution of all the particles at the time t		
	$2X$	$2X_{R_1} + 2X_{R_2} + 2X_{R_3}$	

References

- Amirante, R., Cassone, E., Distaso, E., Tamburrano, P., 2017. Overview on recent developments in energy storage: mechanical, electrochemical and hydrogen technologies. *Energy Convers. Manage.* 132, 372–387. doi.org/10.1016/j.enconman.2016.11.046.
- Ashby, M.F., Polyblank, J., first published January 2012. Materials for Energy Storage Systems – A White Paper. University of Cambridge. Materials for Energy Storage Systems, Granta Teaching Resources, Version 2.0.
- Baes, C.F., Mesmer, R.S., 1976. *The Hydrolysis of Cations*. Wiley, New York.
- Brooker, R.P., Bell, C.J., Bonville, L.J., Kunz, H.R., Fenton, J.M., 2015. Determining vanadium concentrations using the UV-Vis response method. *J. Electrochem. Soc.* 162 (4), A608–A613. https://doi.org/10.1149/2.0371504jes.
- Cheng, M., 1991. *Electrolyte Optimization and Studies for the Vanadium Redox Flow Battery*. Master Thesis. University of New South Wales, Australia.
- Choi, Nak Heon, Kwon, Soon-kwan, Kim, Hansung, 2013. Analysis of the oxidation of the V(II) by dissolved oxygen using UV-Visible spectrophotometry in a Vanadium Redox Flow Battery. *J. Electrochem. Soc.* 160, A973–A979. https://doi.org/10.1149/2.145306jes.
- Choi, Chanyong, Kim, Soohyun, Kim, Riyul, Choi, Yunsuk, Kim, Soowhan, Jung, Ho-young, Hoon Yang, Jung, Kim, Hee-Tak, 2017. A review of vanadium electrolytes for vanadium redox flow batteries. *Renew. Sustain. Energy Rev.* 69, 263–274. https://doi.org/10.1016/j.rser.2016.11.188.
- Crans, D.C., Smees, J.J., Gaidamauskas, E., Yang, L., 2004. The chemistry and biochemistry of vanadium and the biological activities exerted by vanadium compounds. *Chem. Rev.* 104, 849–902. https://doi.org/10.1021/cr020607t.
- Cunha, A., Martins, J., Rodrigues, N., Brito, F.P., 2015. Vanadium redox flow batteries: a technology review. *Int. J. Energy Res.* 39, 889–918. https://doi.org/10.1002/er.3260.
- Cussler, E.L., 1984. *Diffusion – Mass Transfer in Fluid Systems*, third ed., Cambridge.
- Ding, Y., Chen, H., Cong, T.N., Yang, W., Tan, C., Li, Y., 2009. Progress in electrical energy storage system: a critical review. *Prog. Nat. Sci.* 19, 291–312. https://doi.org/10.1016/j.pnsc.2008.07.014.
- Elvington, K., Keramidas, A.D., Crans, D.C., Pettersson, L., 1998. Speciation in vanadium bioinorganic systems. 5. Interactions between vanadate, uridine, and imidazoles an aqueous potentiometric, 51V, 17O, and 13C NMR study. *Inorg. Chem.* 37 (24), 6153–6160. https://doi.org/10.1021/ic9712333.
- Fassulo, O.T., 1965. *Sulfuric Acid; Use and Handling*. McGraw-Hill, University of Minnesota - New York.

- Fu, Q., Sun, W., 2001. Mie theory for light scattering by a spherical particle in an absorbing medium. *Appl. Opt.* 40 (9), 1354–1361. doi.org/10.1364/AO.40.001354.
- Guzman, J., Saucedo, I., Navarro, R., Revilla, J., Guibal, E., 2002. Vanadium interactions with chitosan: influence of polymer protonation and metal speciation. *Langmuir* 18 (5), 1567–1573. https://doi.org/10.1021/la010802n.
- Ivakin, A.A., Voronova, E.M., 1973. A spectrophotometric study of vanadium (IV) sulfate complexes. *Russ. J. Inorg. Chem.* 18 (7), 956.
- Jiang, Z., Klyukin, K., Alexandrov, V., 2016. Structure, hydrolysis, and diffusion of aqueous vanadium ions from Car-Parrinello molecular dynamics. *J. Chem. Phys.* 145, 114303. doi.org/10.1063/1.4962748.
- Kausar, N., 2002. Studies of V(IV) and V(V) species in vanadium cell electrolyte. April 2002, A thesis submitted as part of the requirements for the degree of Doctor of Philosophy (Ph.D) M.Sc (Chemistry), University of New South Wales, Sydney 2052, Australia.
- Le Flem, G., 1964. *Le système V2O5 – ThO2*. Faculté des Sciences de l'Université de Bordeaux.
- Leung, P., Li, X., Ponce-de-León, C., Berlouis, L., John-Low, C.T., Walsh, F.C., 2012. Progress in redox flow batteries, remaining challenges and their applications in energy storage. *RSC 2*, 10125–10156. https://doi.org/10.1039/c2ra21342g.
- Li, L., Kim, S., Wang, W., Vijayakumar, M., Nie, Z., Cheng, B., Zhang, J., Xia, G., Hu, J., Graff, G., Liu, J., Yang, Z., 2011. A Stable Vanadium Redox Flow Battery with High Energy Density for Large Scale Energy Storage. *Adv. Energy Mater.* 1, 394–400. https://doi.org/10.1002/aenm.201100008.
- Post, K., Robins, R.G., 1976. Thermodynamic diagrams for the vanadium-water system at 298.15K. *Electrochim. Acta* 21 (6), 401–405. https://doi.org/10.1016/0013-4686(76)85115-8.
- Rahman, F., 1998. *Stability and Properties of Supersaturated Vanadium Electrolytes For High Energy Density Vanadium Redox Battery* PhD Thesis. University of New South Wales, Australia.
- Rahman, F., Skyllas-Kazacos, M., 1998. Solubility of vanadyl sulfate in concentrated sulfuric acid solutions. *J. Power Sources* 72 (2), 105–110. doi.org/10.1016/S0378-7753(97)02692-X.
- Rahman, F., Skyllas-Kazacos, M., 2009. Vanadium redox battery: positive half-cell electrolyte studies. *J. Power Sources* 189 (2), 1212–1219. https://doi.org/10.1016/j.jpowsour.2008.12.113.
- Rychcik, M., Skyllas-Kazacos, M., 1988. Characteristics of a new all-vanadium redox flow battery. *J. Power Sources* 22 (1), 59–67. 10.1016/0378-7753(88)80005-3.
- Selbin, J., 1965. The chemistry of oxovanadium (IV). *Chem. Rev.* 65 (2), 153–175. https://doi.org/10.1021/cr60234a001.
- Skyllas-Kazacos, M., Rychcik, M., Robins, R., 1988. All-vanadium redox battery. US4786567.
- Skyllas-Kazacos, M., Cao, L., Kazacos, M., Kausar, N., Mousa, A., 2016. Vanadium electrolyte studies for the vanadium redox battery—a review 9(13), 1521–1543. doi.org/10.1002/cssc.201600102.
- Skyllas-Kazacos, M., Kim, K.J., Park, M.S., Kim, Y.J., Kim, J.H., Dou, S.X., 2015. A technology review of electrodes and reaction mechanisms in vanadium redox flow batteries. *J. Mater. Chem. A* 3, 16913–16933. https://doi.org/10.1039/C5TA02613j.
- Skyllas-Kazacos, M., Milne, N.A., Kazacos, G.C., 2007. Membrane properties and behaviour in the Generation 2 Vanadium Bromide Redox Flow batteries. *Mater. Forum* 32, 72–77.
- Skyllas-Kazacos, M., Parasuraman, A., Lim, T.M., Menictas, C., 2013. Review of material research and development for vanadium redox flow battery applications. *Electrochim. Acta* 101, 27–40. doi.org/10.1016/j.electacta.2012.09.067.
- Sum, E., Rychcik, M., Skyllas-Kazacos, M., 1985. Investigation of the V(V)/V(IV) system for use in the positive half-cell of a redox battery. *J. Power Sources* 16 (2), 85–95. https://doi.org/10.1016/0378-7753(85)80082-3.
- Sum, E., Skyllas-Kazacos, M., 1985. A study of the V(II)/V(III) redox couple for redox flow cell applications. *J. Power Sources* 15 (2), 179–190. https://doi.org/10.1016/0378-7753(85)80071-9.
- Thaller, L.H., 1974. Electrically rechargeable redox flow cells. Bibliographic Code: 1974ieec.conf.924T. Published. In: Intersociety Energy Conversion Engineering Conference, 9th, San Francisco, Calif., August 26–30, 1974, Proceedings. (A75–10476 01–44) New York, American Society of Mechanical Engineers, p. 924–928.
- Thaller, L.H., Jan. 01, 1977. Redox flow cell development and demonstration project. NASA Tech. Memo.-79067; Document ID: 19790016274; Accession Number: 79N24445.
- Vijayakumar, M., Li, Liyu, Graff, Gordon, Liu, Jun, Zhang, Huamin, Yang, Zhenguo, Hu, Jian Zhi, 2011. Towards understanding the poor thermal stability of V5+ electrolyte solution in Vanadium Redox Flow Batteries. *J. Power Sources* 196 (7), 3669–3672. https://doi.org/10.1016/j.jpowsour.2010.11.126.
- Vijayakumar, M., Wang, W., Nie, Z., Sprenkle, V., Hu, J., 2013. Elucidating the higher stability of vanadium(V) cations in mixed acid based redox flow battery electrolytes. *J. Power Sources* 241, 173–177. https://doi.org/10.1016/j.jpowsour.2013.04.072.
- Wallace, R.M., 1966. Determination of the second dissociation constant in sulfuric acid by Donnan Membrane Equilibrium. *J. Phys. Chem.* 70 (12), 3922–3927. https://doi.org/10.1021/j100884a029.
- Wang, W., Luo, Q., Li, B., Wei, X., Li, L., Yang, Z., 2013. Recent progress in redox flow battery research and development. *Adv. Funct. Mater.* 23 (8), 970–986. https://doi.org/10.1002/adfm.201200694.